Laser and Particle Beams (2017), *35*, 505–512.

doi:10.1017/S0263034617000489

X-ray and ion emission studies from subnanosecond laser-irradiated SiO_2 aerogel foam targets

C. KAUR,[1,2] S. CHAURASIA,[1] A.A. PISAL,[3] A.K. ROSSALL,[4] D.S. MUNDA,[1] A. VENKATESWARA RAO,[3] AND M.N. DEO[1]

[1]High Pressure and Synchrotron Radiation Physics Division, Bhabha Atomic Research Centre, Mumbai – 400085, India
[2]Homi Bhabha National Institute, Anushaktinagar, Mumbai – 400 094, India
[3]Air Glass Laboratory, Department of Physics, Shivaji University, Kohlapur – 416 004, Maharashtra, India
[4]International Institute for Accelerator Applications, University of Huddersfield HD1 3DH, UK

(Received 27 March 2017; Accepted 10 June 2017)

Abstract

In this experiment, a comparative study of ion and X-ray emission from both a SiO_2 aerogel foam and a quartz target is performed. The experiment is performed using Nd:glass laser system operated at laser energy up to 15 J with a pulse duration of 500 ps with focusable intensity of 10^{13}–10^{14} W/cm^2 on target. X-ray fluxes in different spectral ranges (soft and hard) are measured by using X-ray diodes covered with Al filters of thickness 5 μm (0.9–1.56 keV) and 20 μm (3.4–16 keV). A 2.5 times enhancement in soft X-ray flux (0.9–1.56 keV) and a decrease of 1.8 times in hard X rays (3.4–16 keV) for 50 mg/cc SiO_2 aerogel foam is observed compared with the solid quartz. A decrease in the flux of the *K*-shell line emission spectrum of soft X rays is noticed in the case of the foam targets. The high-resolution *K*-shell spectra (He-like) of Si ions in both the cases are analyzed for the determination of plasma parameters by comparing with FLYCHK simulations. The estimated plasma temperature and density are $T_c = 180$ eV, $n_e = 7 \times 10^{20}$ cm^{-3} and $T_c = 190$ eV, $n_e = 4 \times 10^{20}$ cm^{-3} for quartz and SiO_2 aerogel foam, respectively. To measure the evolution of the plasma moving away from the targets, four identical ion collectors are placed at different angles (22.5, 30, 45, and 67.5°) from target normal. The angular distribution of the thermal ions are scaled as $\cos^n\theta$ with respect to target normal, where n = 3.8 and 4.8 for the foam and quartz, respectively. The experimental plasma volume measured from the ion collectors and shadowgraphy images are verified by a two-dimensional Eulerian radiative–hydrodynamic simulation (POLLUX code).

Keywords: X rays from laser-produced plasma; Aerogel targets; X-ray enhancement

1. INTRODUCTION

The production of small, compact, easily accessible, and short pulse length X-ray sources from laser plasma interactions has significantly facilitated research in advanced science, such as radiobiology, X-ray microscopy, microlithography, astrophysical and fusion applications, measurement of the opacity of materials, X-ray-driven shock studies for equation-of-state (EOS) measurements of materials under extreme conditions, and time-resolved X-ray diffraction of materials (Lewis & Mcglinchey, 1984; Chaker *et al.*, 1988; Förstera *et al.*, 1989; O'Neill *et al.*, 1989; Lindl, 1995; Rischel *et al.*, 1997; Daido, 2002; Borisenko *et al.*, 2008; Keiter *et al.*, 2008; Loupias *et al.*, 2009; Rossall *et al.*, 2010; Grant, 2016). The demand for high X-ray fluxes in practical applications has triggered extensive research for the enhancement of the X-ray yield of laser-produced plasmas (LPP) (Rosmej *et al.*, 2015). However, the conversion efficiency of laser energy to X ray from the solid targets is low due to the reflection of most of the laser light near the critical density surface. For a large X-ray yield, absorption of the laser energy inside the target should be high. Therefore, to enhance the X-ray yield, various laser conditions (power density, pulse duration, and wavelength) and target properties have been tested previously. For example, to enhance the X-ray yield, the use of a prepulse (Andreev *et al.*, 2002), defocusing the laser to increase the plasma volume (Chaurasia *et al.*, 2013), structured targets (Nishikawa *et al.*, 2001), gas targets (Fiedorowicz *et al.*, 2000), and low-density targets (Borisenko *et al.*, 2013) have been used. The use of low-density targets has been proven as a prominent candidate for the enhancement of X-ray emission

Address correspondence and reprint requests to: S. Chaurasia, High Pressure & Synchrotron Radiation Physics Division, Purnima Building, Bhabha Atomic research Centre, Trombay, Mumbai-400085, India. E-mail: shibu@barc.gov.in

from LPP. Many targets, such as gold foam (Shang *et al.*, 2013), hydrocarbon-based foam (Chaurasia *et al.*, 2015), carbon foam (Chaurasia *et al.*, 2010*a*, *b*), structured surfaces (Rajeev *et al.*, 2003; Krishnamurthy *et al.*, 2015), porous Si (Nishikawa *et al.*, 1997), agar–agar foam (Limpouch *et al.*, 2006), are used for this purpose. A considerable amount of work has been done already for X-ray enhancement using metal-doped (Ti and Ge) low-density silicon oxide foam targets (Fournier *et al.*, 2004, 2009). In the previous work (Shang *et al.*, 2013), the X-ray conversion efficiency in the case of gold foam was found to increase by 1.34 times as compared with solid gold in the range of multi-eV to multi-keV due to a larger absorption of laser light via inverse bremsstrahlung. Further (Nishikawa *et al.*, 2001) by using ultrashort laser pulse, the penetration depth was found to increase in the case of porous Si targets, which results in a reduction of threshold of prepulse for enhancement of X-ray intensity. Earlier investigation in our laboratory (Chaurasia *et al.*, 2010*a*, *b*) indicated an enhancement in the soft X ray by a factor of 1.8 and 2.3 in carbon foam and Pt-doped carbon foam, respectively, when compared with the solid carbon.

The enhancement of soft X rays from the foam target is attributed to the underdense nature of the target, which allows the laser to burn through the target supersonically. In this paper, we have made a contribution in the above area of research by studying X ray and ion emission from SiO_2 aerogel foam targets simultaneously with optical shadowgraphy of the plasma. The procedure of preparing of foam targets is also briefly described.

2. EXPERIMENTAL SETUP

The laser system used in these experiments is a 15 J/500 ps Nd:glass laser with intensity 10^{13}–2×10^{14} W/cm^2 available at BARC, Mumbai, India. The high-power laser is focused to a focal spot of 100 μm on the target using a f/5 lens and placed in an experimental chamber evacuated to 4×10^{-5} mbar. The schematic of experimental setup is shown in Figure 1. Targets used are solid quartz and 50 mg/cc pure SiO_2 aerogel foam and also along with (25% CH_3 + 75% SiO_2) foam of 60 and 40 mg/cc densities. The continuum X-ray flux (free–free and free–bound) in the soft X-ray (0.8–1.56 keV) and the hard X-ray (3.4–16 keV) spectral range are measured using silicon photodiodes covered with 9 and 20 μm aluminum foils, respectively. The time-integrated X-ray line emission spectra were recorded by dispersing the X rays with a flat TAP (Thallium Acid Phthalate) crystal (2d = 25.75 Å) on to an X-ray CCD camera (M/s Rigaku made, Model-X-vision 4M, Czech Republic) placed at 45° to the target normal. Four identical ion collectors are placed at different angles, that is, 22.5, 30, 45, and 67.5° with respect to the target normal and laser axis to measure the plasma evolution and its size. The details of the crystal spectrometer and ion collectors are described somewhere else (Kaur *et al.*, 2017). To study the dynamic motion of the plasma and its volume, a transverse two-frame optical shadowgraphy system was developed. The magnification at the focal plane of the imaging lens was 3.45 with a spatial resolution of 12 μm and a temporal resolution of 500 ps. The details of the shadowgraphy system are reported elsewhere (Chaurasia *et al.*, 2010).

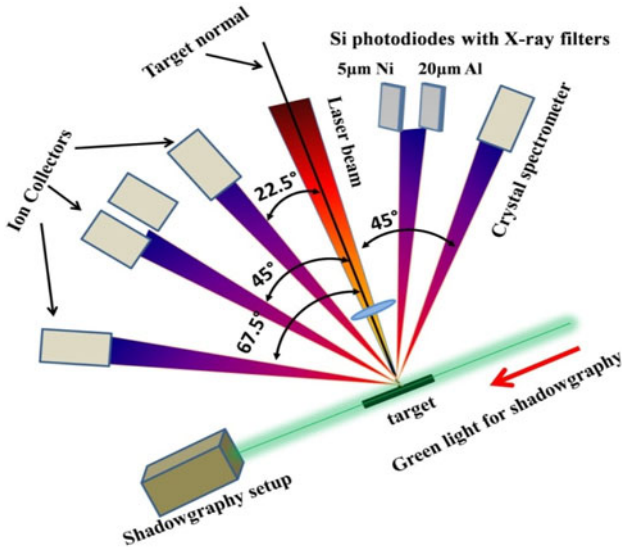

Fig. 1. Schematic of various X-ray and ions diagnostics used in experiment.

3. METHOD OF PREPARATION OF SIO_2 FOAM TARGETS

The preparation of silica aerogel mainly includes three steps: gel preparation, aging of the gel, and drying of the gel. The aerogel (i.e., silica foam targets) is prepared by the sol–gel process followed by supercritical drying in which tetramethoxysilane (TMOS) is the source of silica. In the first step, the hydrolysis of TMOS is done by adding 0.001 M oxalic acid to initiate polymerization. As the TMOS is only partially miscible with water, alcohol (methanol) is added as a solvent to this solution to ensure the same phase for the reaction to occur. Ammonium hydroxide is used as a catalyst to increase the condensation reaction speed. To obtain the low-density silica aerogels, the molar ratio of TMOS:MeOH:H_2O was kept constant at 1:12:4. All the solutions (silicon alkoxide, solvent, water, and catalyst) were mixed in a 100 ml Pyrex beaker, and the resulting sols were immediately transferred to Pyrex test tubes and closed air tight. After gelation, the resulting alcogels were covered with methanol to prevent the shrinkage and cracking of the wetgels. All of the alcogels were supercritically dried in an autoclave to obtain the low-density silica aerogels. The 25% CH_3 and 75% silica aerogels (foam targets) were produced by using the methyltrimethoxy precursor in the place of TMOS precursor, and followed the same procedures in making the aerogels. The MTMS precursor was diluted with methanol and hydrolyzed using the 0.001 M oxalic acid. After 12 hours of hydrolysis, the condensation of

https://doi.org/10.1017/S0263034617000489 Published online by Cambridge University Press

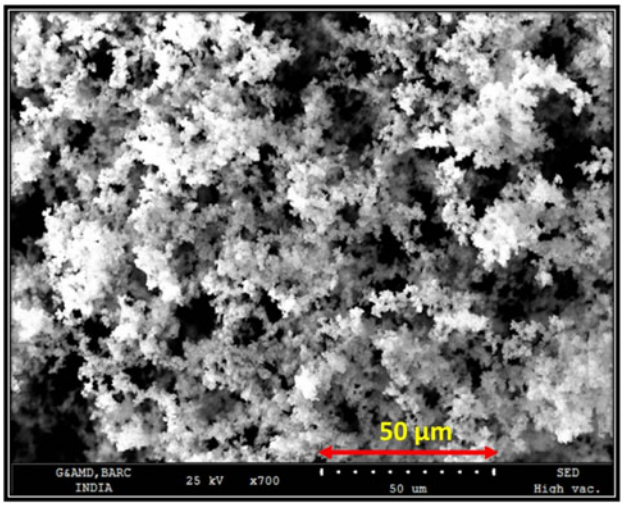

Fig. 2. SEM image of 50 mg/cc pure silica aerogel foam with 25 kV electron beam and ×700 magnification.

the resulting methyl modified silica sol (25% CH_3 and 75% silica) was carried out using 13 M ammonium hydroxide. The 60 mg/cc and 40 mg/cc MTMS based aerogel were obtained by keeping the molar ratios of MTMS: Methanol: water at 1:20:4 and 1:34:4, respectively. The acidic and basic catalysts were added in the form of water. More details are given on the preparation of the silica aerogels elsewhere (Pajonk *et al*., 1997; Rao *et al*., 1998, 2003, 2006). The scanning electron microscope (SEM) image of 50 mg/cc silica aerogel foam is shown in Figure 2.

4. RESULTS AND DISCUSSION

4.1. Effect of target densities on soft and hard X-ray yields

When an intense laser focuses on a target, a highly dense and hot plasma is produced. The emitted radiations are in the X-ray spectral region. There are three mechanisms of production of X rays in plasma, that is, free–free, free–bound, and bound–bound (Eliezer, 2002). The laser wavelength, pulse duration, and choice of target material strongly affect the X-ray yield (conversion factor of laser pulse to X rays). In our case, we measured the X-ray radiation due to free–free and free–bound transitions using X-ray photodiodes covered with different filters to measure the soft and hard X rays. The output of the photodiode signals for the soft and hard X rays are plotted with respect to the laser intensity in Figure 3a, 3b, respectively. From the figures, it can be seen that the X-ray flux (I_x) scales with the laser intensity (I_L) at a constant pulse duration and wavelength as $I_x = (I_L)^{\alpha}$, where α is constant. However, the value of α is calculated by slope of the graph plotted between $\ln(I_x)$ versus $\ln(I_L)$ and found to be 1 and 0.5 for quartz and SiO_2 aerogel foam targets, respectively, in case of soft X rays. However, in the case of hard X rays, these values are 0.9 and 0.6 for quartz and SiO_2 aerogel foam targets, respectively. It is observed that the soft X-ray emission (0.9–1.56 keV) from the low-density (50 mg/cc) SiO_2 aerogel foam is almost 2–2.5 times higher than in solid quartz for almost all of the investigated laser intensities and decreases with increase of the foam density. The X-ray yield from 70 mg/cc pure SiO_2 is lying in

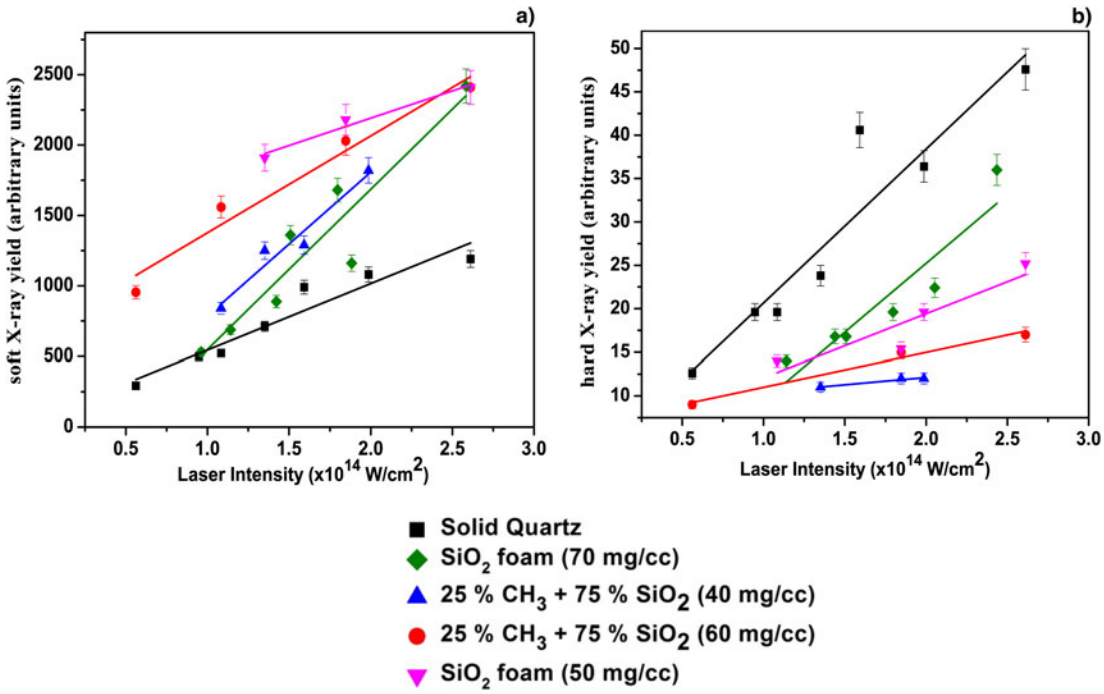

Fig. 3. Comparison of (a) soft X-ray flux and (b) hard X-ray flux from solid quartz with SiO_2 aerogel foam of various densities, such as 50 mg/cc, 25% CH_3 + 75% SiO_2 aerogel foam of 60 and 40 mg/cc densities.

https://doi.org/10.1017/S0263034617000489 Published online by Cambridge University Press

between solid quartz and 50 mg/cc pure SiO_2 aerogel foam target. However, in the case of hard X-ray emission (3.4–16 keV), the flux from low-density SiO_2 aerogel foam is ~1.8 times lower than the yields from the solid quartz. The X-ray flux from the silica foam with composition (25% CH_3 + 75% SiO_2) of densities 60 and 40 mg/cc are also measured. It is observed that the soft X-ray yield from these targets are slightly lower than the pure SiO_2 aerogel foam target of density 50 mg/cc and at the same time higher than the X-ray yield from the quartz target.

The enhancement of soft X-ray emission in the low-density foam target is mainly due to two reasons. Firstly, it is due to lower losses to hydrodynamic phenomenon (shock formation), and secondly and more prominently it is due to volumetric heating. Xu *et al.* (2011) have done simulation studies using a one-dimensional (1D) multigroup radiation hydrodynamic code and have shown that in the case of a subcritically dense plasma, it is heated supersonically and no shock wave formation takes place, while in an overdense plasma, the percentage loss of energy increases with the target density and is at maximum for the solid targets. Secondly, the enhancement of the volume of the X-ray emission is due to the initial penetration of the laser due to the transparency. The dynamics of laser light absorption in low-density porous material is explained by a long inhomogeneous period during which there exists a stochastic distribution in the low-density region in the plasma. As a result, the radiation is absorbed in a volume at the so-called geometrical transparency length, which is determined by the classical collision mechanism (Bugrov *et al.*, 1997), as given in following equation:

$$L_T = \frac{9.2 \times 10^{-8}}{Z} \left(\frac{A}{Z}\right)^2 \frac{T^{3/2}}{\lambda^2 \cdot \rho^2}. \quad (1)$$

Here A and Z are the atomic number and charge of the plasma ions, respectively, λ is the wavelength of the laser light (μm), T is the electron temperature (keV), and ρ is the plasma density (g/cm^3). From the above equation, it can be seen that the penetration depth and hence the volume of plasma is inversely proportional to the square of the density. The same can be seen from the shadowgraphs for the quartz (Fig. 4a–4c) and for 50 mg/cc SiO_2 aerogel foam targets (Fig. 4d–4f) at a delay times of 2 and 8 ns after the arrival of the main laser pulse on targets. From Figure 4c, 4f, it can be seen that after 8 ns of the arrival of incident laser, the lateral plasma size in the SiO_2 aerogel foam case is 1.35 times larger than the solid quartz. It can also be seen from Figure 4d (without laser), 4e (2 ns delay), and 4f (8 ns delay) that the heated volume is larger inside the targets (shown with dotted circles). However, in the case of quartz, the interaction is only at the solid surface.

We also recorded the time-integrated spectrum of ions from LPP with the help of ions collectors placed at four different angles from target normal (i.e., at 22.5, 30, 45, and 67.5°) to verify the volumetric heating concept. The angular distribution of the amplitude of the thermal ions (plasma) are plotted in Figure 5, for two different laser shots of same

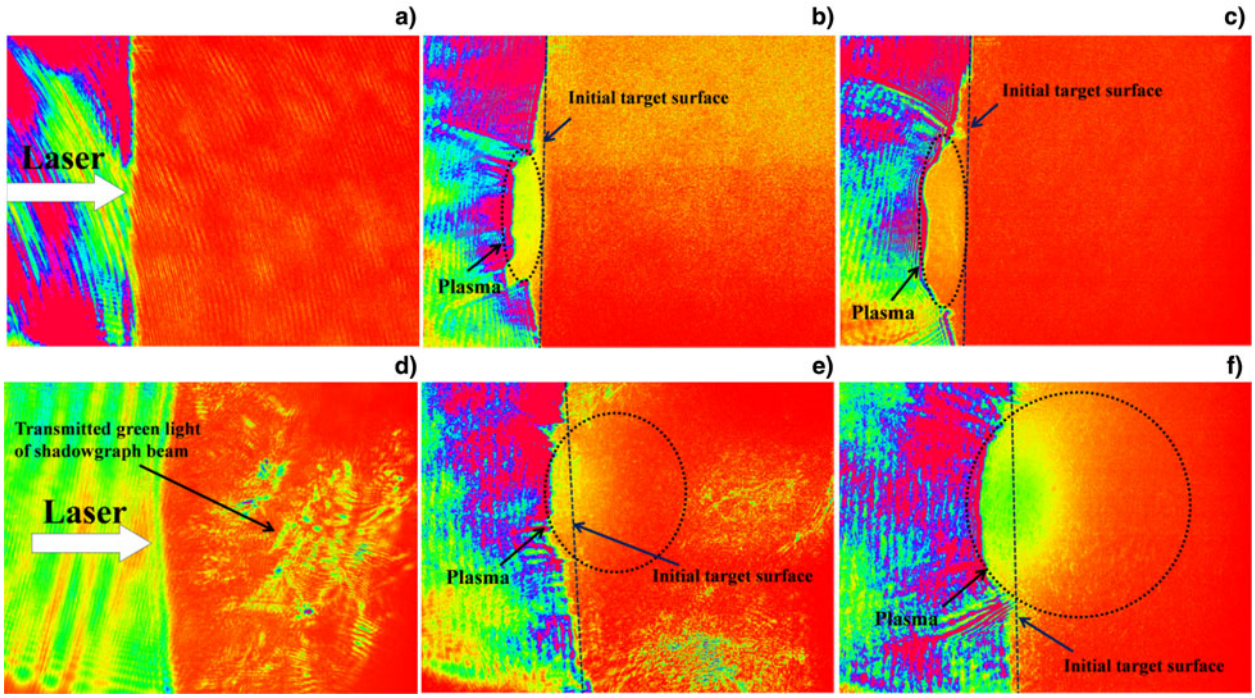

Fig. 4. Shadowgraph of solid quartz (a) at $t = 0$ ns, (b) at $t = 2$ ns, and (c) at $t = 8$ ns after laser pulse on the targets, and for foam targets at (d) $t = 0$ ns, (e) at $t = 2$ ns, and (f) at $t = 8$ ns after laser pulse on the targets. The dotted circle in each image is showing the region of plasma.

https://doi.org/10.1017/S0263034617000489 Published online by Cambridge University Press

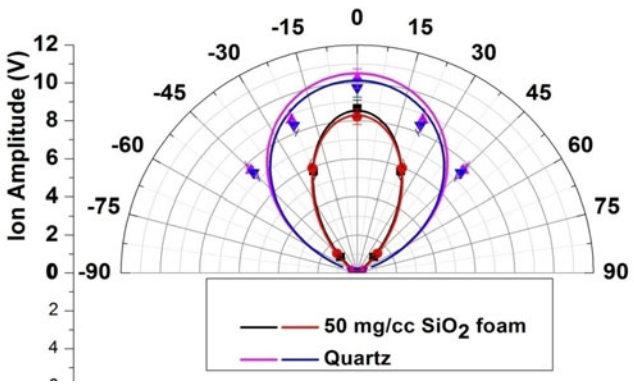

Fig. 5. Angular distribution of the thermal ion flux from the 50 mg/cc SiO_2 aerogel foam and quartz targets for two laser shots of approximately same energy.

energies on the targets of 50 mg/cc SiO_2 aerogel foam and quartz target. The angular distribution of the thermal ions are scaled as $P(\theta) = P(0)\ \cos^n\theta$, where $n = 3.8$ and 4.8 for the foam and quartz targets, respectively. It can be seen from Figure 5, that the thermal ion flux from the foam target is larger and closer to isotropic (hence the larger volume) compared with the thermal ion flux from the quartz. A similar behavior has been observed via theoretical simulation done by our group using 2D Eulerian radiative–-hydrodynamic code POLLUX, which is briefly described in the next section.

4.2. Simulation results to verify the volume effect

The 2D Eulerian radiative–hydrodynamic code POLLUX was originally developed to model moderate irradiance (10^{10} W/cm^2) optical and infrared laser irradiation of a solid target and the subsequently produced strongly ionized plasma, which further interacts with the incident laser beam. The code solves the three first-order quasi-linear partial differential equations of hydrodynamic flow using the flux-corrected transport model of Boris & Book (1976), with an upwind algorithm (Courant *et al.*, 1952) for the first term. The energy is absorbed by the plasma electrons through inverse bremsstrahlung and distributed through electron–ion collisions, the equilibration of which is determined by the Spitzer plasma collision rate (Spitzer & Härm, 1953). For calculation of the EOS variables, POLLUX utilizes in-line hydrodynamic EOS subroutines from the Chart-D (Thompson, 1970) EOS package developed at Sandia National Laboratories, Livermore, CA, USA. This code uses an explicit solver; therefore, a Courant number of ~1 has been used to increase stability where the Courant number (C) is given by

$$C = \frac{u_x \Delta t}{\Delta x} + \frac{u_y \Delta t}{\Delta y} \sim 1, \tag{2}$$

where u_x and u_y are magnitudes of the particle velocities in the respective directions, Δt is the time step, and Δx and Δy are the cell spatial dimensions. The ionization and level populations are calculated assuming local thermodynamic equilibrium, an assumption which is justified for hydrodynamic time scales (>1 ps).

To enable the ray tracing of the incident laser pulse within the code, the Eulerian mesh is subdivided into triangular cells with the Eulerian mesh center points at the triangle corners allowing for the refractive index and associated gradient within each cell to be calculated via direct differencing. The refractive index is continuous across cell boundaries and assumes a linear electron density variation within each cell. The (x, y) trajectory of each ray in the cell is then assumed to be parabolic dependent upon the refractive index (n_0) and its derivative (n_1), given by,

$$y^2 = 4\left(\frac{n_0}{n_1}\right)x. \tag{3}$$

The parameters used in the code were a p-polarized laser intensity of 1×10^{14} W/cm^2 incident onto solid quartz with a density of 2.65 g/cm^3 and silica foam with a density of 50 mg/cm^3.

The contour plot for the electron density and electron temperature at $t = 1$ ns after the start of the laser pulse are shown in Figure 6. It can be seen from Figure 6 that the plasma expansion differs greatly between the two targets with the foam targets creating much larger lower density plasma. It proves that the enhancement is due to a volume effect where the foam target has a much greater volume of emitting plasma, which is in consistent with the results obtained by shadowgraphy and the ion collector.

4.3. Estimation of plasma parameters with *K*-shell spectra

The K-shell spectra of silicon in quartz and SiO_2 aerogel foam targets are recorded with the help of TAP crystal spectrometer as shown in Figure 7a, 7b. The crystal spectrometer is optimized to measure the He-α line ($1s^2$–$1s2p$), the intercombination line ($1s^2\ ^1S_0$–$1s2p^3P_1$), and the Li-like satellite of He-α line ($1s^22p$–$1s2p^2$). These lines are important for determination of the plasma temperature and density. The plasma temperature and density are estimated by taking into account the ratio of the dielectronic satellite of He-α line (i.e., $1s^22p$–$1s2p^2$) to its parent resonance line, that is, He-α line($1s^2$–$1s2p$) and intercombination line ($1s^2\ ^1S_0$–$1s2p^3P_1$) to He-α ($1s^2\ ^1S_0$–$1s2p^1P_1$), respectively. For determination of temperature and density, simulation is carried out using the FLYCHK software (Chung *et al.*, 2005), which generates a synthetic spectrum that is matched with the experimental data after several iterations for a range of temperatures and densities. The experimental spectra matched with FLYCHK for He-like lines of the silicon in the quartz target at $T_c = 180$ eV, $T_h = 1000$ eV, $f = 0.009$, $n_e = 7 \times 10^{20}$ cm^{-3}, and for SiO_2 aerogel foam at $T_c = 190$ eV, $T_h = 800$ eV, $f = 0.01$, and $n_e = 4 \times 10^{20}$ cm^{-3} as shown in

https://doi.org/10.1017/S0263034617000489 Published online by Cambridge University Press

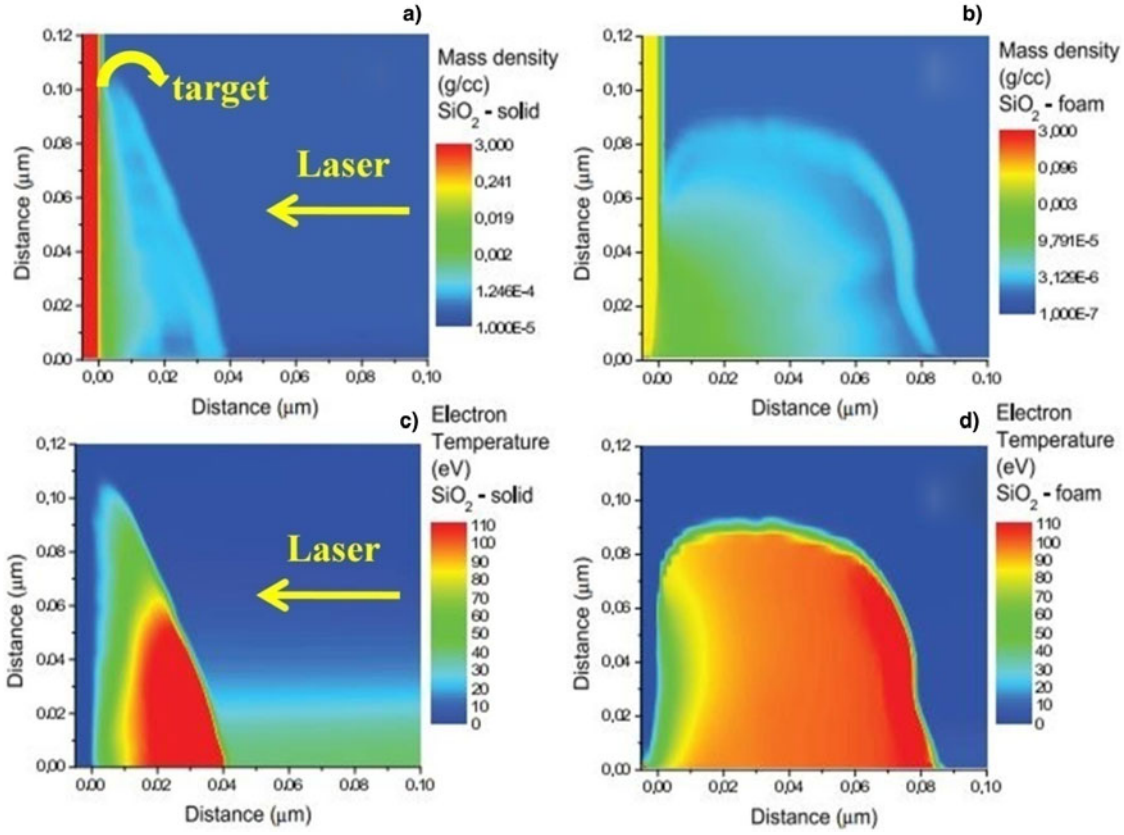

Fig. 6. (a, b) Contour plots for solid quartz and SiO_2 aerogel foam for electron density and (c, d) for electron temperature after a delay of $t = 1$ ns with respect to the start of the laser pulse on the target.

Figure 7a, 7b, where T_c and T_h are the cold and hot electron temperatures, respectively, f is the hot to cold component fraction and n_e is the electron density. The amplitude of the line emission is lower in the case of the foam target, which is due to a lower plasma density as can be seen from simulation results where the density of the foam plasma is 4×10^{20} cm^{-3}. The hot electron temperature is lower and the value of f is higher in the case of foam targets, which indicates lower hard X-ray emission than the solid quartz as shown in Figure 3b.

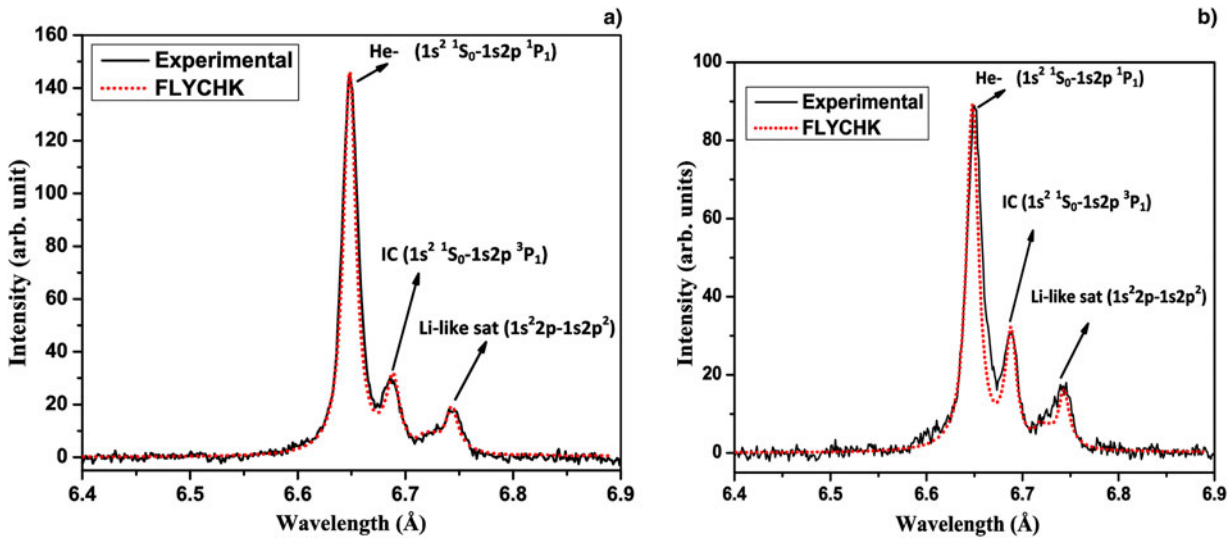

Fig. 7. Experimental spectrum matched with FLYCHK for He-like lines of the silicon in the (a) quartz at $T_c = 180$ eV, $T_h = 1000$ eV, $f = 0.009$, and $n_e = 7 \times 10^{20}$ cm^{-3} and (b) SiO_2 aerogel foam at $T_c = 190$ eV, $T_h = 800$ eV, $f = 0.01$, and $n_e = 4 \times 10^{20}$ cm^{-3}.

https://doi.org/10.1017/S0263034617000489 Published online by Cambridge University Press

4.4. Conclusions

A comparison of soft and hard X rays flux from quartz and low-density SiO_2 aerogel foam targets is done. Pure SiO_2 aerogel foam with density 50 and 70 mg/cc, and (25% CH_3 + 75% SiO_2) of densities 60 and 40 mg/cc are used. Two X-ray diodes with different filters are used to examine X-ray emission in soft (0.9–1.56 keV) and hard X-ray (3.4–16 keV) regions. An enhancement of 2.5 times in soft X-ray emission and a decrease of 1.8 times in hard X-ray emission for 50 mg/cc SiO_2 aerogel foam is observed compared with the solid quartz. The ion collector's data show that, the ion flux from the solid quartz is found to be more directional, whereas from SiO_2 aerogel foam, it is nearly isotropic. This behavior was attributed to the volume effect, which has been further verified by shadowgraph profiles of the plasma plume at two different time scales during the plasma evolution (2 and 8 ns) and simulation. Simulations with a 2D hydrodynamic code POLLUX supported the indication of volume heating of plasma being the cause for the change in X-ray emission. For determination of the plasma temperature and density, the spectra including He-like resonance line along with satellites and intercombination of Si plasma were matched with synthetic spectrum generated by using FLYCHK for both quartz and 50 mg/cc SiO_2 aerogel foam targets. The calculated plasma parameters are T_c = 180 eV, $T_h = 1000$ eV, $f = 0.009$, and $n_e = 7 \times 10^{20}$ cm^{-3} and $T_c = 190$, $T_h = 800$ eV, $f = 0.01$, and $n_e = 4 \times 10^{20}$ cm^{-3} for quartz and SiO_2 aerogel foam, respectively.

ACKNOWLEDGMENTS

The authors from BARC wish to acknowledge the support and continuous encouragement received from Dr. S. M. Sharma, former Director, Physics group and Dr. N. K. Sahoo, Director, Physics Group, BARC. Also, we acknowledge the excellent support given by Mr. C. G. Murali, Mrs P. Leshma and Mr Ritesh Sable in design and implementation of laser electronics and smooth operation of laser system. Dr. Venkateswara Rao is highly thankful to the University Grants Commission (UGC), New Delhi, Government of India, for the UGC-Basic Science Research (BSR) Faculty Fellowship. Dr. A. A. Pisal acknowledges the stipendiary grant received from the UGC.

REFERENCES

Andreev, A.A., Limpouch, J., Iskakov, A.B. & Nakano, H. (2002). Enhancement of X-ray line emission from plasmas produced by short high-intensity laser double pulses. *Phys. Rev. E* **65**, 026403.

Boris, J.P. & Book, D.L. (1976). Flux-corrected transport. III. Minimal-error FCT algorithms. *J. Comput. Phys*. **20**, 397–431.

Borisenko, N.G., Bugrov, A.E., Burdonskiy, I.N., Fasakhov, I.K., Gavrilov, V.V., Goltsov, A.Y., Gromov, A.I., Khalenkov, A.M., Kovalskii, N.G., Merkuliev, Y.A. & Petryakov, V.M. (2008). Physical processes in laser interaction with porous low-density materials. *Laser Part. Beams* **26**, 537–543.

Borisenko, N.G., Chaurasia, S., Dhareshwar, L.J., Gromov, A.I., Gupta, N.K., Leshma, P., Munda, D.S., Orekhov, A.S., Tripathi, S. & Merkuliev, Y.A. (2013). Laser study into and explanation of the direct-indirect target concept, in EPJ Web of Conf., vol. 59, 03014. EDP Sciences.

Bugrov, A.E., Gus'kov, S.Y., Rozanov, V.B., Burdonskii, I.N., Gavrilov, V.V., Gol'tsov, A.Y., Zhuzhukalo, E.V., Koval'skii, N.G., Pergament, M.I. & Petryakov, V.M. (1997). Interaction of a high-power laser beam with low-density porous media. *J. Exp. Theor. Phys*. **84**, 497–505.

Chaker, M., Pépin, H., Bareau, V., Lafontaine, B., Toubhans, I., Fabbro, R. & Farsi, B. (1988). Laser plasma X-ray sources for microlithography. *J Appl. Phys*. **63**, 892–899.

Chaurasia, S., Leshma, P., Murali, C.G., Borisenko, N.G., Munda, D.S., Orekhov, A., Gromov, A.I., Merkuliev, Y.A. & Dhareshwar, L.J. (2015). Studies on subcritical and overcritical density laser ablated TAC foam targets. *Opt. Commun*. **343**, 1–5.

Chaurasia, S., Leshma, P., Tripathi, S., Murali, C.G., Munda, D.S., Sharma, S.M., Kailas, S., Gupta, N.K. & Dhareshwar, L.J. (2010*a*). Simultaneous measurement of particle velocity and shock velocity for megabar laser driven shock studies. *BARC Newslett*. **317**, 13–21.

Chaurasia, S., Tripathi, S., Leshma, P., Murali, C.G. & Pasley, J. (2013). Optimization of bremsstrahlung and characteristic line emission from aluminum plasma. *Opt. Commun*. **308**, 169–174.

Chaurasia, S., Tripathi, S., Munda, D.S., Mishra, G., Murali, C.G., Gupta, N.K., Dhareshwar, L.J., Rossall, A.K., Tallents, G.J., Singh, R. & Kohli, D.K. (2010*b*). Laser interaction with low-density carbon foam. *Pramana* **75**, 1191–1196.

Chung, H.K., Chen, M.H., Morgan, W.L., Ralchenko, Y. & Lee, R.W. (2005). FLYCHK: generalized population kinetics and spectral model for rapid spectroscopic analysis for all elements. *High Energy Density Phys*. **1**, 3–12.

Courant, R., Isaacson, E. & Rees, M. (1952). On the solution of nonlinear hyperbolic differential equations by finite differences. *Commun. Pure Appl. Math*. **5**, 243–255.

Daido, H. (2002). Review of soft X-ray laser researches and developments. *Rep. Prog. Phys*. **65**, 1513.

Eliezer, S. (2002). *The Interaction of High-power Lasers with Plasmas*. Bristol: IOP .

Fiedorowicz, H., Bartnik, A., Jarocki, R., Rakowski, R. & Szczurek, M. (2000). Enhanced X-ray emission in the 1-keV range from a laser-irradiated gas puff target produced using the double-nozzle setup. *Appl. Phys. B* **70**, 305–308.

Förstera, E., Gäbel, K. & Uschmanna, I. (1989). X-ray microscopy of laser-produced plasmas with the use of bent crystals. *Laser Part. Beams* **9**, 135–148.

Fournier, K.B., Constantin, C., Poco, J., Miller, M.C., Back, C.A., Suter, L.J., Satcher, J., Davis, J. & Grun, J. (2004). Efficient multi-keV X-ray sources from Ti-doped aerogel targets. *Phys. Rev. Lett*. **92**, 165005.

Fournier, K.B., Satcher, J.H., May, M.J., Poco, J.F., Sorce, C.M., Colvin, J.D., Hansen, S.B., Maclaren, S.A., Moon, S.J., Davis, J.F. & Girard, F. (2009). Absolute X-ray yields from laser-irradiated germanium-doped low-density aerogels. *Phys. Plasmas* **16**, 052703.

Grant, A. (2016). Foam mitigates key obstacle in quest for laser fusion. *Phys. Today* **69**, 22.

Kaur, C., Chaurasia, S., Poswal, A.K., Munda, D.S., Rossall, A.K., Deo, M.N. & Sharma, S.M. (2017). K-shell X-ray

spectroscopy of laser produced aluminum plasma. *J. Quant. Spectrosc. Radiat. Transf.* **187**, 20.

Keiter, P.A., Comely, A., Morton, J., Tierney, H., Workman, J. & Taylor, M. (2008). Conversion efficiency of high-Z backlighter materials. *Rev. Sci. Instrum.* **79**, 10E918.

Krishnamurthy, M., Kundu, M., Bane, K., Lad, A.D., Singh, P.K., Chatterjee, G., Kumar, G.R. & Ray, K. (2015). Enhanced X-ray emission from nano-particle doped bacteria. *Opt. Express* **23**, 17909–17922.

Lewis, C.L.S. & Mcglinchey, J. (1984). Quasi-monocromatic, projection radiography of dense laser driven spherical targets. *Opt. Commun.* **53**, 179–186.

Limpouch, J., Borisenko, N.G., Demchenko, N.N., Gus'kov, S.Y., Kasperczuk, A., Khalenkov, A.M., Kondrashov, V.N., Krousky, E., Kuba, J., Masek, K. & Merkul'ev, Y.A. (2006). Laser absorption and energy transfer in foams of various pore structures and chemical compositions. *Proc. J. Phys. IV* **133**, 57–459.

Lindl, J. (1995). Development of the indirect-drive approach to inertial confinement fusion and the target physics basis for ignition and gain. *Phys. Plasmas* **2**, 3933–4024.

Loupias, B., Perez, F., Benuzzi-Mounaix, A., Ozaki, N., Rabec, M. & Gloahec, L.E. (2009). Highly efficient, easily spectrally tunable X-ray backlighting for the study of extreme matter states. *Laser Part. Beams* **27**, 601–609.

Nishikawa, T., Nakano, H., Ahn, H., Uesugi, N. & Serikawa, T. (1997). X-ray generation enhancement from a laser-produced plasma with a porous silicon target. *Appl. Phys. Lett.* **70**, 1653–1655.

Nishikawa, T., Nakano, H., Oguri, K., Uesugi, N., Nakao, M., Nishio, K. & Masuda, H. (2001). Nanocylinder-array structure greatly increases the soft X-ray intensity generated from femtosecond-laser-produced plasma. *Appl. Phys. B* **73**, 185–188.

O'neill, F., Turcu, I.C.E., Tallents, G.J., Dickerson, J., Lindsay, T., Goodhead, D.T., Stretch, A., Wharton, C.W. & Meldrum, R.A. (1989). A repetitive laser-plasma X-ray source for radiobiology research. *Proc. SPIE 1140, X-Ray Instrumentation in Medicine and Biology, Plasma Physics, Astrophysics, and Synchrotron Radiation*, Paris, France, 1232.

Pajonk, G.M., Rao, A.V., Sawant, B.M., Parvathy, N.N. & Sawant, B.M. (1997). Dependence of monolithicity and physical properties of TMOS silica aerogels on gel aging and drying conditions. *J. Non-Cryst. Solids* **209**, 40–50.

Rajeev, P.P., Taneja, P., Ayyub, P., Sandhu, A.S. & Kumar, G.R. (2003). Metal nanoplasmas as bright sources of hard X-ray pulses. *Phys. Rev. Lett.* **90**, 115002.

Rao, A.V., Bhagat, S.D., Hirashima, H. & Pajonk, G.M. (2006). Synthesis of flexible silica aerogels using methyltrimethoxysilane (MTMS) precursor. *J. Colloid Interface Sci.* **300**, 279–285.

Rao, A.V., Kulkarni, M.M., Amalnerkar, D.P. & Seth, T. (2003). Superhydrophobic silica aerogels based on methyltrimethoxysilane precursor. *J. Non-Cryst. Solids* **330**, 187–195.

Rao, A.V., Pajonk, G.M., Haranath, D. & Wagh, P.B. (1998). Effect of sol-gel processing parameters on optical properties of TMOS silica aerogels. *J. Mater. Synth. Process.* **6**, 37–48.

Rischel, C., Rousse, A., Uschmann, I., Albouy, P.A., Geindre, J.P., Audebert, P., Gauthier, J.C., Fröster, E., Martin, J.L. & Antonetti, A. (1997). Femtosecond time-resolved X-ray diffraction from laser-heated organic films. *Nature* **390**, 490–492.

Rosmej, O.N., Suslov, N., Martsovenko, D., Vergunova, G., Borisenko, N., Orlov, N., Rienecker, T., Klir, D., Rezack, K., Orekhov, A. & Borisenko, L. (2015). The hydrodynamic and radiative properties of low-density foams heated by X-rays. *Plasma Phys. Control. Fusion* **57**, 094001.

Rossall, A.K., Gartside, L.M.R., Chaurasia, S., Tripathi, S., Munda, D.S., Gupta, N.K., Dhareshwar, L.J., Gaffney, J., Rose, S.J. & Tallents, G.J. (2010). X-ray back-lighter characterization for iron opacity measurements using laser-produced aluminium K-alpha emission. *J. Phys. B, At. Mol. Opt. Phys.* **15**, 155403.

Shang, W., Yanga, J. & Dong, Y. (2013). Enhancement of laser to X-ray conversion with a low density gold target. *Appl. Phys. Lett.* **102**, 094105.

Spitzer Jr., L. & Härm, R. (1953). Transport phenomena in a completely ionized gas. *Phys. Rev.* **89**, 977.

Thompson, S.L. (1970). Improvements in the chart d radiation-hydrodynamic code i: analytic equations of state (No. SC-RR–70-28). Sandia Labs., Albuquerque, N. Mex.

Xu, Y., Zhu, T., LI, S. & Yang, J. (2011). Beneficial effect of CH foam coating on X-ray emission from laser-irradiated high-Z material. *Phys. Plasmas* **18**, 053301.

https://doi.org/10.1017/S0263034617000489 Published online by Cambridge University Press